

Complex Microwave Permittivity of Secondary High Explosives

Amanda L. Higginbotham Duque,^{*[a]} William Lee Perry,^[a] and Christine M. Anderson-Cook^[a]

Abstract: We aim to understand how microwaves interact with high explosives by studying the complex permittivity from 1–18 GHz of HMX, RDX, TNT, TATB, PETN, Octol, Comp B, 95% RDX/5% Viton A (PBX-RDX), PBX 9404, PBXN-5, PBXN-7, PBXW-14, PBX 9501, and PBX 9502. The combination of a resonant cavity perturbation technique for determining the room-temperature complex dielectric constant at discrete frequencies and a wide band open circuit method (1–18 GHz) provides an accurate, broadband measurement that describes the dielectric properties in the frequency range of interest. While the values of the real and

imaginary permittivity components did not vary significantly as a function of frequency, we found the real part of the permittivity to be highly dependent on relatively small changes in the material density. We used dielectric mixing theory, specifically the linear-law approximation, to compare the predicted values based on the dielectric properties of individual components with those of the resulting formulation measured experimentally for a select number of samples; the prediction agrees well within the observed variability of the experimentally measured values.

Keywords: Microwaves • Dielectric properties • High explosives

1 Introduction

High explosives are an important class of energetic materials (EMs) used extensively not only in weapons systems, but also the mining and demolition industries. Understanding their physical properties, including interaction with a wide range of electromagnetic radiation frequencies, is essential to proper use and full utilization of their capabilities. The vast amount of electromagnetic energy present in a given situation – especially in a military setting – necessitates the understanding of these interactions, especially in the microwave (MW) region (1000–30,000 MHz). The wavelength of MW radiation deeply penetrates typical energetic materials (meters), allowing the radiation to affect the entire volume of reasonable sized objects. However, little is known about how explosives interact with MW energy; such information is particularly useful for applications such as detection and avoiding inadvertent ignition of high explosives.

The complex permittivity (dielectric constant) of a given homogeneous material is described by real and imaginary components that are both frequency and temperature dependent. The real component (ϵ') is associated with the ability of the dielectric material to store electric energy, while the imaginary component (ϵ''), sometimes referred to as the loss factor, is associated with the dielectric loss (or energy dissipation) that occurs in the material. Therefore, the dielectric properties of a material govern electromagnetic radiation reflection, transmission, absorption, and scattering; furthermore, they are critical to understanding the thermal response during radiation exposure. Permittivi-

ty is often expressed as a relative value: ϵ_r : $\epsilon = \epsilon_0 \epsilon_r = \epsilon_0 (\epsilon' - j\epsilon'')$, where $\epsilon_0 \approx 8.854 \times 10^{-12} \text{ F m}^{-1}$; all permittivity values reported herein are relative to vacuum. Equation (1) and Equation (2) are the Helmholtz and heat equations, respectively:


$$-\nabla^2 E = \omega^2 \epsilon_0 (\epsilon' - j\epsilon'') E \quad (1)$$

$$\rho c (\partial T / \partial t) = k \nabla^2 T + \dot{q}_d \quad (2)$$

where E is the electric field, ω is the angular frequency, ρ is the density, c is the constant pressure specific heat, k is the thermal conductivity, and T is temperature.

Solutions of the Helmholtz equation provide the electromagnetic wave propagation behavior in a medium defined by the complex permittivity, as shown. The dependence of the thermal behavior is shown by the heat equation, which includes a volumetric source term that depends on the loss factor (Equation (3)). Thus, these dielectric properties are required for any accurate computational prediction of the electromagnetic and thermal response (including direct

[a] A. L. Higginbotham Duque, W. L. Perry, C. M. Anderson-Cook
Los Alamos National Laboratory
Los Alamos, NM, USA
*e-mail: aduque@lanl.gov

 Supporting information for this article is available on the WWW under <http://dx.doi.org/10.1002/prop.201300032> or from the author.

thermal ignition) of these materials to radiation exposure in this frequency range.

$$+\dot{q}_d = \omega \varepsilon'' (E^2/2) \quad (3)$$

There has been limited dielectric property characterization of high explosives explored in the literature. We previously reported the complex permittivity of TATB powder at two different densities from 1–18 GHz [1], while Hasue et al. reported the single frequency complex permittivity of a few energetic materials at approx. 60% theoretical maximum density (TMD) [2]. Naval researchers have made measurements of a select few explosives and oxidizers from 1–6 GHz (data not published), and there are some reports for the dielectric properties of HMX (8.3 GHz) [3], PETN, and TNT (34.5 GHz) [4] as a function of density. However, to date a comprehensive report for continuous wide range frequency measurements of complex permittivity for common high explosives does not exist. Furthermore, correlation of the results to density variations and comparison to an applicable dielectric mixing model has not been reported.

Here, we report the room-temperature dielectric properties of HMX, RDX, TNT, TATB, PETN, Octol, Comp B, 95% RDX/5% Viton A (PBX-RDX), PBX 9404, PBXN-5, PBXN-7, PBXW-14, PBX 9501, and PBX 9502. The measurements were made using a twofold approach; the combination of a resonant cavity perturbation technique for determining the complex dielectric constant at discrete frequencies (2.5 and 13.3 GHz) and a wide band (1–18 GHz) open circuit method provide an accurate, broadband measurement that describes the dielectric properties in the frequency range of interest. Additionally, select samples prepared at difference densities were compared at a single frequency to illustrate the density effect and determine a functional dependence. Finally, the measurement results of some single-component samples (HMX, TATB, RDX, Kel-F, Viton A, Estane, and BDNPA/F) were incorporated into the linear-law dielectric mixing approximation [5] to estimate the effective permittivity of solid-solid mixtures (i.e. explosive binder systems) at 2.5 and 13.3 GHz. These calculated values were compared to those found experimentally for several polymer-bonded explosives (PBX).

2 Experimental Section

2.1 Materials and Sample Preparation

All explosive powders were unmodified and used as received from the standard supplying ammunition plant. The PBX materials were used in molding powder form; the content of each PBX formulation is given in Table 1.

Cavity perturbation measurements were performed on sample powders pressed into cylindrical pellets measuring 3.2 mm (diameter) × 6.4 mm (height). A hardened steel die was used in a pneumatic press; each pellet was held for 3 minutes at a pressure of 41,500 Pa at ambient temperature. The density of each pellet was carefully calculated by measuring the dimensions with high precision calipers and recording the mass. The importance of density on the dielectric properties is discussed in Section 3.1.1.

Samples for the open circuit method were prepared by hand-pressing the powders directly into the coaxial fixture. (NOTE and word of caution: special precaution was taken for safety; a custom-made plastic plunger was used that had been designed to fit into the fixture without creating friction; inadvertent ignition of an energetic material in this confined configuration could lead to a violent explosion.) The highest possible hand pressed density was achieved by adding small quantities of powder to the fixture and using the plunger to press the material down to the bottom. The density was calculated by recording the mass of the fixture with and without sample powder, and measuring the volume of space occupied by the sample.

2.2 Cavity Perturbation

The cavity perturbation method is well studied and proves to be effective at measuring the dielectric parameters of materials [6,7]. This technique utilizes the presence of a small amount of material to perturb the resonant frequency and quality factor (Q) of the cavity. When a small dielectric sample is inserted in the cavity, the resonant frequency shift and change in bandwidth is measured. Simple analysis is then used to determine the complex permittivity at the resonant frequency. If the perturbation is a sphere having a volume much smaller than the cavity volume and the cavity fill permittivity is taken to be 1, the following relationships apply [5,8]:

Table 1. Polymer bonded explosive (PBX) formulations and their contents.

PBX 9502	PBXN-7	PBXW-14	PBX 9404	PBX 9501	PBXN-5	PBX-RDX	Octol	Comp B
95% TATB 5% Kel-F	60% TATB 35% RDX 5% Viton A	50% HMX 45% TATB 5% Viton A	94% HMX 3% NC ^a 3% CEF ^b	95% HMX 2.5% Estane 2.5% NP ^c	95% HMX 5% Viton A	95% RDX 5% Viton A	75% HMX 25% TNT	60% RDX 40% TNT

a) NC = nitrocellulose; b) CEF = tris(beta)-chloroethylphosphate (plasticizer); c) NP = nitroplasticizer: eutectic mixture of bis(2,2-dinitropropyl) acetal and bis(2,2-dinitropropyl) formal (BDNPA/F)

$$\frac{\omega_{0c} - \omega_{0s}}{\omega_{0c}} = (\epsilon'_s - 1)C(V_s/V_c) \quad (4)$$

$$\frac{1}{Q_s} - \frac{1}{Q_c} = \epsilon''C(V_s/V_c) \quad (5)$$

$$Q = (1 + \beta)^*(\omega_{0c}/\Delta\omega) \quad (6)$$

$$\beta = \frac{1}{(d_2/d) - 1} \quad (7)$$

$$C = \sqrt{\frac{9\epsilon''}{(\epsilon'_s + 2)^2 + \epsilon''^2}} \approx \frac{3}{\epsilon'_s + 2} \quad (8)$$

where ω is the resonant frequency of the cavity with and without the sample inserted, V is the volume of the cavity and the sample, and $\Delta\omega$ is the half-power bandwidth as determined from the S -parameters in the frequency domain. The subscript '0' refers to the resonant condition, 'c' refers to the empty cavity, and 's' refers to the cavity perturbed by the sample. C is related to the electric field perturbation inside the cavity when the sample is introduced; the value will vary depending on the sample dimensions, permittivity, and location within the cavity [5]. The quality factor of the empty cavity (Q_c) is related to the quality factor of the loaded cavity (Q_s) by a coupling coefficient (β), which describes the coupling between the resonator and the external measurement circuit. The coupling coefficient is determined from the diameter of the "resonant circle" (d) and the diameter of the loss circle (d_2) in the polar domain [8]. The approximation made in Equation (8) is valid for a bulk resistivity less than about $1 \text{ } \Omega\text{m}$ because it leads to a value for dielectric loss that is small relative to the real permittivity ($\epsilon'' \approx \sigma/\omega\epsilon_0$, where σ is the bulk conductivity) [5].

For our materials of interest, spherical samples cannot be easily produced and inserted into a cavity; instead cylindrical samples were used. Thus, a simple analytical form for C does not exist. To eliminate uncertainties due to sample size, geometry, and location in the cavity, we used calibration standards that have an identical geometry and real permittivity near that of the material of interest [9]. The cavity is a $9 \text{ cm} \times 9.2 \text{ cm}$ diameter copper cylinder (as shown in Figure 1). It has a fundamental frequency of 2.5 GHz (TM₀₁₀) and several higher order modes, viewable up to 20 GHz (the limit of the network analyzer, Agilent Technologies N5320A PNA-L).

The samples were pressed into cylinders near theoretical maximum density (TMD); they were then inserted into the cavity through a hole along the centerline (see Figure 1b, c). The insertion depth was precisely controlled using a micrometer stage and a laser/diode system to reproducibly determine the initial sample position prior to insertion, so that the inserted volume is known. Three calibration standards with dielectric constants of 2.1 (Teflon), 5.7 (Macor), and 9.4 (alumina) were used to find C for those dielectric

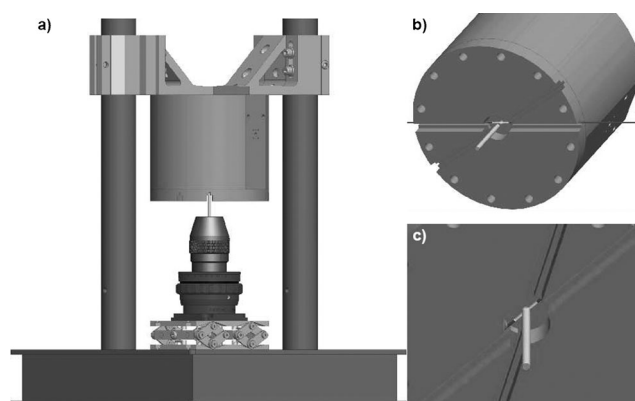


Figure 1. Experimental setup for performing cavity perturbation measurements. Image (a) shows an overview of the setup, with the micrometer stage controlling sample insertion depth; b) View of the cavity with the sample insertion hole and laser guide; c) A pressed sample being introduced into the cavity.

constants over a range of insertion depths. The value for Teflon is generally accepted, and the values for alumina and Macor were previously measured by inserting the sample/standard along the full axis length of the cavity. For this configuration, with the assumption that the sample radius is much smaller than the cavity radius, an analytic method exists to compute the dielectric constant.

At a given insertion depth, the fit function used was:

$$\frac{\omega_{0c} - \omega_{0s}}{\omega_{0c}} = (\epsilon'_s - 1)\{A/(2 + B\epsilon'^n)\}(V_s/V_c) \quad (9)$$

where C has been substituted for an expression containing ϵ'_s and the fit coefficients B , n , and A ; the sample-to-cavity volume ratio is estimated to be 16×10^{-6} . The coefficients B , n , and A are used to fit a plot of normalized frequency shift vs. real permittivity at a given insertion depth using the known values of the three calibration standards above in addition to air. The initial guesses are: $B=0.1$, $A=20$, and $n=1$. Note that this fit function is functionally consistent with the exact analytic expression for a sphere. Figure 2 shows an example plot of normalized frequency shift vs. real permittivity at four different insertion depths, each plotted with the respective fit function. The real permittivity of the unknown sample of interest was then interpolated based on the fit function and measured normalized frequency shift. Four different specimens were measured for each sample at each frequency, and average values are reported in the following section.

2.3 Open-Circuit

The details of the open-circuit technique have been covered in a previous publication [1], and will only be briefly described here. This technique is effective for measuring the broadband dielectric properties of low-loss, low-density

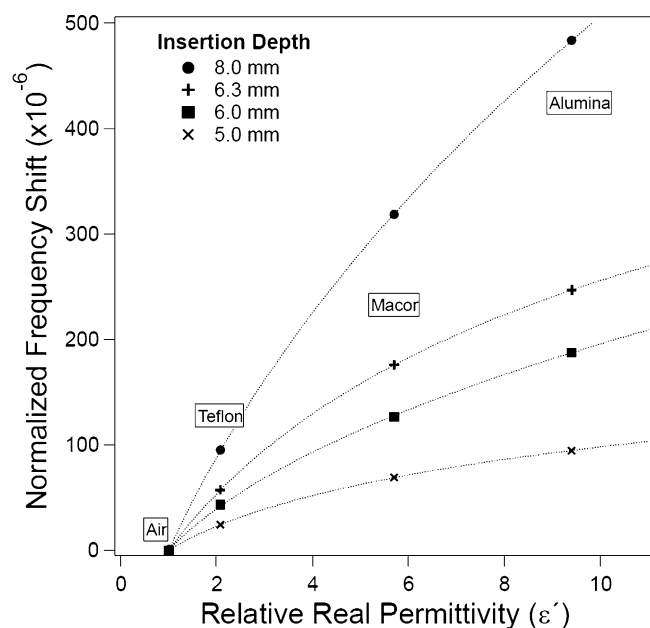


Figure 2. Response of the cavity perturbation setup for three standard materials (alumina, Macor, and Teflon) and air as a function of insertion depth. The real permittivity of unknown materials is determined by interpolation using the measured normalized frequency shift and the fit function generated by the standards at the appropriate insertion depth.

air-particle mixtures from the reflection coefficient (scattering parameters, S_{11}) of the sample-loaded fixture. For the test fixture, an Amphenol Precision Connector – 7 mm (APC-7) shielded open circuit coaxial line was used (Figure 3). The instrument was calibrated prior to each use using a standard coaxial calibration kit that included open, short, and load terminations. Powdered samples were carefully hand-pressed into the fixture (see Section 2.1), and the S_{11} data of both the empty and filled fixture were obtained on a calibrated Agilent Technologies N5320A PNA-L vector network analyzer. The real and imaginary parts of the permittivity were calculated with a mathematical model of the test fixture [10]. Because the hand-pressed powders will never reach the near-theoretical maximum densities of the cylindrical pellets used for cavity perturbation, the air-powder mixtures measured with the open circuit method are expected to have a lower real permittivity. This is corrected for by finding the complex dielectric constants at several discrete frequencies using the high-density samples and the cavity perturbation technique; a correction on the broadband spectrum obtained with the less-dense powders may then be performed.

Supporting Information (see footnote at the first page of this article): Complete tabulated results of cavity perturbation and open circuit coax measurements, as well as broadband dielectric properties (full-spectrum graphs) and discussion of BDNPA/F, ethanol, and hexane.

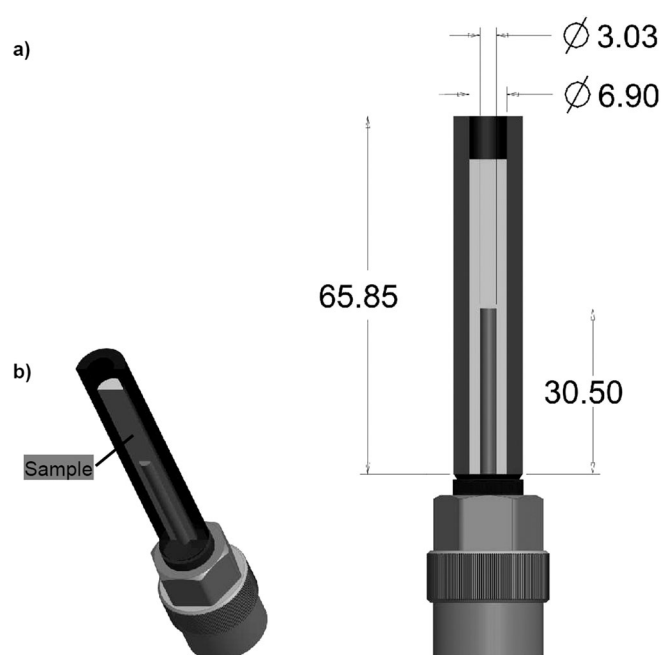


Figure 3. a) Experimental apparatus for performing open-circuit measurements. b) The sample volume fill around the center conductor is highlighted; c) Coaxial fixture dimensions given in millimeters.

3 Results and Discussion

3.1 Dielectric Properties Measurement Results

A summary of the results for all room-temperature data collected is given in Figure 4. The data are overlaid for both the cavity perturbation (single points) and open circuit (traces) methods; the combination of these techniques provides an accurate, wide-band complex permittivity measurement. The cavity perturbation measurements were made at 2.50 GHz and 13.25 GHz; broadband data from the open circuit method were taken continuously between 1–18 GHz. Note that the broadband data (real permittivity only) are corrected for density using the values obtained on the same samples near TMD from the cavity perturbation method. The imaginary component of permittivity does not appear to vary significantly with changes in density within experimental error; further discussion on density dependency will follow. A Table containing all numerical values of these results is located in the Supporting Information.

The dielectric response of solid materials depends strongly on material phase and lattice structure. The degree of crystallinity, existence of permanent dipoles, mobility of free charge, and defects all contribute to dielectric response [11]. In addition, inherent differences in the dielectric properties between materials may be traced to differences in the magnitude of the molecular polarizability. This reflects the strength with which the nuclear charges control the electron distributions and prevent their distur-

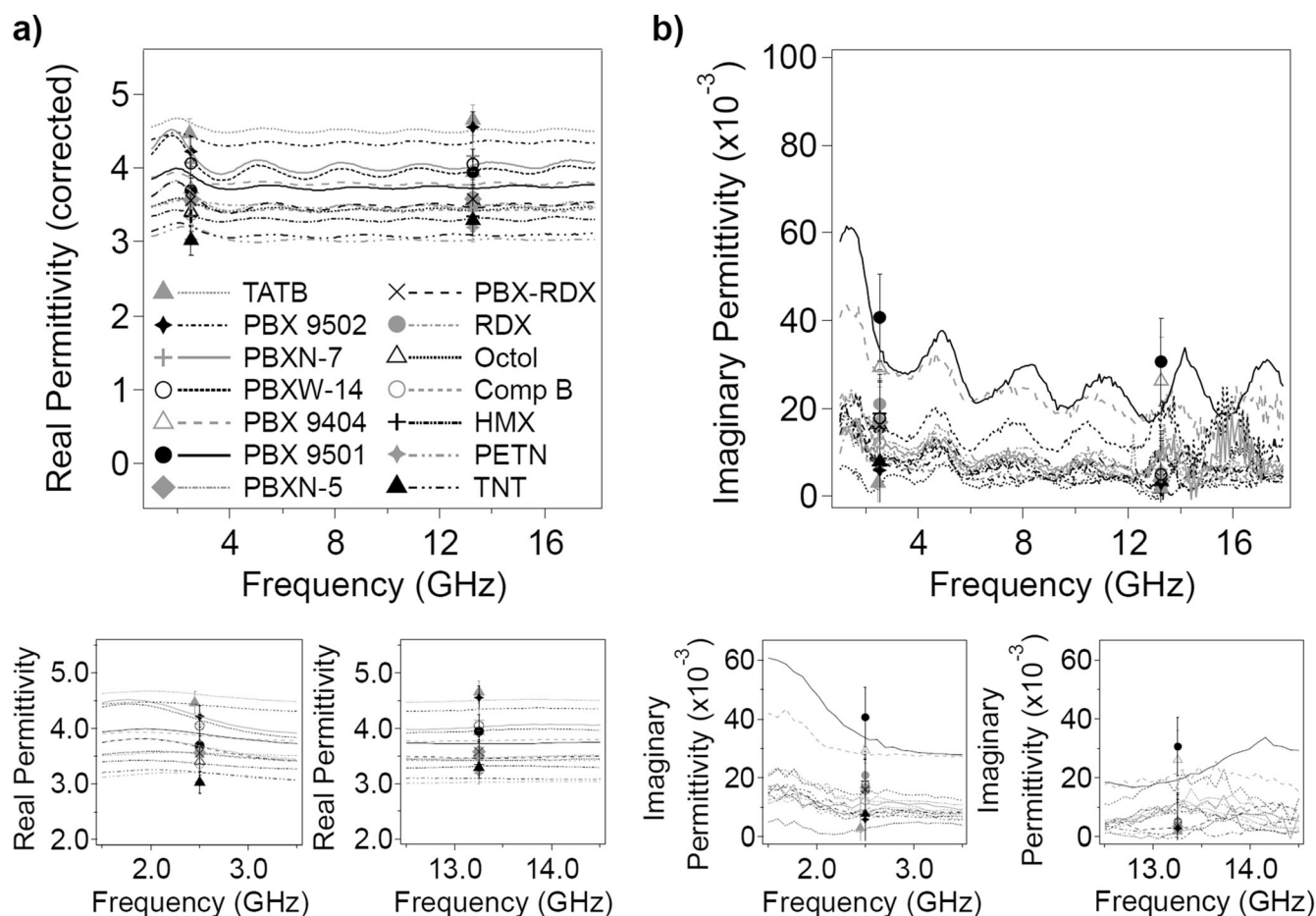


Figure 4. Summary of all dielectric property data results. a) Corrected real permittivity as a function of frequency. b) Imaginary permittivity as a function of frequency. The bottom panels are zoomed regions centered on the frequencies of the cavity perturbation measurements. All of the data are listed in Table format in the Supporting Information.

tion by the applied field. If the molecule has few electrons, their distribution is tightly controlled by the nuclear charges and polarizability is low. If the molecule contains large atoms with electrons some distance from the nucleus, the nuclear control is less, the electron distribution is more diffuse, and the polarizability is greater [12].

In general, all the materials we measured demonstrated constant behavior of the real permittivity as a function of frequency in the range studied. The imaginary permittivity followed this same trend, with more pronounced oscillations observed in the data. These oscillations may be attributed to artifacts in the instrument response and do not reflect actual fluctuations in the material; the measured values may be interpolated as the average across the frequency range. The artifacts arise from the measurement procedure, which compares the response of an empty fixture to the sample-loaded fixture result. Small changes in the fixture dimensions that occur while pressing the material into the fixture will cause a reflection phase error.

TATB and formulations that contain TATB have the highest values of real permittivity, ranging from $\epsilon'_{\text{avg}} = 4.6$ (pure

TATB) to $\epsilon'_{\text{avg}} = 4.1$ (PBXW-14, 45% TATB). Formulations containing energetic material plus at least 5% binder or plasticizer followed with intermediate values of real permittivity from $\epsilon'_{\text{avg}} = 3.8$ (PBX 9404) to $\epsilon'_{\text{avg}} = 3.6$ (PBX-RDX). Materials showing the lowest values for real permittivity were pristine energetics (other than TATB) and/or mixtures of two or more energetics. RDX was the highest of the other pristine materials ($\epsilon'_{\text{avg}} = 3.5$) while TNT and PETN were the lowest ($\epsilon'_{\text{avg}} = \text{approx. } 3.2$). The measured values for HMX ($\epsilon'_{\text{avg}} = 3.4$ at 86% TMD) agree well with previously reported values for HMX at similar conditions [3]. Values for TNT up to 10 GHz have been reported by von Hippel ($\epsilon' = 2.9$) [9], however no information is given on sample state (i.e. flakes vs. crystals) or density. We attribute the lower von Hippel value to a lower sample density.

TATB and TATB-containing formulations show a distinctly higher real permittivity than the other organic explosives tested, which may be partially attributed to adsorbed water content. TATB is known to adsorb water quite readily [13], and it has been shown that less than 0.5% water content will increase the real permittivity by 0.5–1 [14]. Although

the TATB was dried in a vacuum oven before pressing, the pellets were stored in the open atmosphere for several days prior to testing; therefore, slight water content ($< 1\%$) is likely the cause of the consistently higher real permittivity values for TATB-containing samples. In fact, when our data is correlated to that collected by Pyper (dielectric constant vs. moisture content), it appears our TATB samples contain approximately 0.2% water. We are not yet clear if adsorbed water plays a similarly important role in the other explosive solids that we studied; however, the other materials (especially PBX formulations) are more resistant to water adsorption in the open atmosphere. Nevertheless, dry TATB has a reported dielectric constant of around 4 [14], which is still significantly higher than the other pristine samples ($\epsilon'_{\text{avg}} = 3.1\text{--}3.5$). These differences may be attributed to inherent differences in the molecular polarizability, discussed above.

The polymer-bonded explosive (PBX) samples with approximately 3 wt.-% of a polar plasticizer component (i.e. PBX 9501 with a eutectic mixture of bis(2,2-dinitropropyl) acetal/formal (BDNPA/F) and PBX 9404 with tris(beta-chloroethylphosphate)) had real permittivity values higher than the PBX formulations that did not contain plasticizer. However, the samples with a polymeric binder with polar components (i.e. PBX-RDX and PBXN-5 with 5% Viton A) had a slightly lower real permittivity value than those containing TATB and/or plasticizer, but still were significantly higher than pristine HMX and RDX.

The trend for imaginary permittivity or loss factor, however, is quite different. The materials with the highest loss values contained binder and a polar plasticizer component (PBX 9501 and 9404), followed by composites with at least 5% of the binder Viton A (PBX-RDX, PBXW-14, PBXN-5, and PBXN-7). The neat materials and PBX 9502 had the lowest values of imaginary permittivity. These observations are expected because the dominant loss mechanism in the 1–18 GHz frequency range is dipolar or reorientation polarization. The loss occurs primarily with materials that contain polar components; the influence of a changing electric field induces redistribution of permanent dipoles in a molecule that results in greater dielectric loss than for nonpolar materials [15].

3.1.1 Effect of Density

The density of a sample is critical to consider when reporting values for real permittivity, as also reported by Glancy and Cawsey [3,4]. The broadband data (1–18 GHz) was collected on samples approximately 65–75% TMD; the average real permittivities calculated on these samples were found to be approximately 65–75% of the real permittivity values measured using the cavity perturbation technique on near-TMD pressed pellets (95–98% TMD). Thus, the correlation between density and observed real permittivity values appears to be roughly linear, which agrees with previous studies [3,4]. In addition, because our samples have

low dielectric contrast with air “inclusions” (which corresponds to density changes), a linear approximation of dielectric properties with density near TMD is valid [5]. More discussion follows in Section 3.2 regarding the use of mixing theory with air as a mixing component to estimate dielectric properties with variations in density.

We further investigated the relationship between density and real permittivity with the more accurate cavity perturbation method. We prepared a series of samples with slight intentional variations in the density, controlled by differences in the pressing conditions. For example, the maximum densities obtained were pressed using the maximum allowed conditions on the pneumatic press/die system. However, if the pressure and/or time held are reduced, the resulting pellet has a lower density. A representative plot of the results for PBX 9501 is shown in Figure 5, and the tabulated data are given in Table 2. It is evident that some materials are more sensitive to density variations (i.e. PBX 9404 and PBX 9501), but the majority of neat materials behave similarly, especially given the allowed error range. The predicted real permittivity value at TMD of the respective material is also given, assuming a linear trend through the data points. Further detail on the methods and confidence intervals for extrapolation of real permittivity values at TMD is given in the next section. The differences in values between those measured and predicted at TMD (up to 10% in some cases) highlight the importance of reporting material density when considering the real permittivity value.

In our measurements, changes in density are not as pronounced for the imaginary component, however. In the

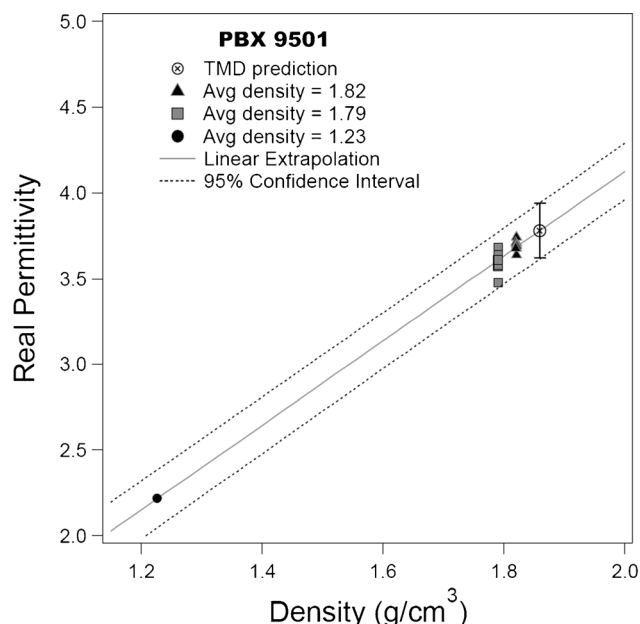


Figure 5. Real permittivity of PBX 9501 as a function of density. A linear extrapolation is used to predict the value at TMD; the error bars represent the 95% confidence interval.

Table 2. Real permittivity as a function of density (measured, error ± 0.2) as well as the predicted real permittivity at TMD.

Material	ρ [g cm ⁻³]	ϵ'
PBX 9501	1.86 ^{a)}	3.78 \pm 0.16
	1.82	3.7
	1.79	3.6
	1.23	2.2
TATB	1.94 ^{a)}	4.79 \pm 0.22
	1.86	4.5
	1.82	4.5
	1.21	2.6
PBX 9404	1.87 ^{a)}	4.08 \pm 0.16
	1.76	3.7
	1.71	3.6
	1.39	2.5
HMX	1.90 ^{a)}	5.00 \pm 0.59
	1.63	3.4
	1.59	3.3
	1.45	2.6
RDX	1.81 ^{a)}	3.93 \pm 0.16
	1.70	3.6
	1.67	3.5
	1.39	2.5
Comp B	1.74 ^{a)}	3.58 \pm 0.16
	1.66	3.4
	1.60	3.2
	1.28	2.2
Octol	1.84 ^{a)}	3.74 \pm 0.23
	1.73	3.4
	1.63	3.3
	1.25	2.3
TNT	1.65 ^{a)}	3.21 \pm 0.17
	1.59	3.0
	1.55	3.0
	1.23	2.0

a) Theoretical maximum density. The corresponding permittivity values were calculated based on the linear regression of all measured data points at three different densities; the error is the 95 % confidence interval.

density variation experiments described above, the imaginary permittivity was also calculated; however, no significant variation was observed within experimental error (data not shown).

3.1.2 Error Analysis

The error in the single frequency cavity perturbation measurements was determined considering internal variations in the experimental apparatus in addition to error analysis calculated on each variable parameter present in Equation (3) and Equation (5). The error in the parameter C (which is a form of the fit function used to calculate ϵ'_{unk}) was solved using the known $\epsilon' = 9.4$ for alumina and the experimental variance in repeated measurements of the normalized frequency shift ($\frac{\omega_{0c} - \omega_{0i}}{\omega_{0c}}$) for this sample (3 %). The error in C was found to be 2.7 %. The error in ϵ'_{unk} was calculated by propagating the errors from the normalized frequency shift

and C (Eqn 9); the error in ϵ'_{unk} was found to be approximately 5 %, resulting in an absolute value of approximately 0.2 for most samples.

The error in ϵ''_{unk} was determined similarly; the error in C and a historical average in fluctuation of the cavity quality factor in a day (0.5 %) were used to propagate the error in ϵ''_{unk} using Eqn 5. Because the absolute values of ϵ''_{unk} are small (< 0.05), the percent error is large (20–30 %). The absolute value of the error for most samples was found to be 0.01.

The error in real and imaginary permittivity data obtained using the open circuit method has been discussed at length [10]. The uncertainty in the real permittivity is dominated by phase uncertainties, and the imaginary part by the magnitude of the reflection coefficient [10]. Using the analysis shown by Baker-Jarvis and taking into consideration our specific measurement set-up, we estimate the error to be 1 %.

In order to evaluate the error in our TMD predictions based on linear extrapolation of the data, we calculated prediction intervals for real permittivity based on the observed density over three specified levels for each of the compounds. Since the observations were obtained over a period of 1–2 days in the laboratory, the unit-to-unit variability of the replicates (observations obtained with nominally the same observed density) is known to underestimate the total variability. These differences are helpful for estimating short term variability, but additional variability needs to be taken into account to capture the long term variability [16]. Based on the experimental error calculated above for the single frequency cavity perturbation measurements, estimates of the long-term variability were obtained. Hence, the 95 % prediction intervals were estimated using the following equation:

$$\hat{y}_0 \pm t_{0.975, n-2} \sqrt{\hat{\sigma}^2 + \hat{\sigma}_{\text{long term}}^2 + \hat{\sigma}^2 (x_0' (X'X)^{-1} x_0)} \quad (10)$$

where \hat{y}_0 is the maximum likelihood estimate of real permittivity based on the simple linear regression model $y = \beta_0 + \beta_1 x + \epsilon$ with ϵ assumed to be normally distributed with mean 0 and variance σ^2 , $t_{0.975, n-2}$ is the 97.5 percentile of a central t-distribution with $n-2$ degrees of freedom (where $n \in [25, 30]$ is the sample size obtained for each compound), $\hat{\sigma}^2$ is the maximum likelihood estimate of σ^2 , $\hat{\sigma}_{\text{long term}}^2$ is the estimated long term variability, and $x_0' (X'X)^{-1} x_0$ is the contribution to the prediction interval based on parameter uncertainty and the location of the new prediction relative to the observed data. The t-distribution is appropriate based on the assumption of Normally distributed observations [17]. Eqn 10 was used to estimate the prediction interval for values between 1.1 and 2 in Figure 5 for PBX 9501 as well as the theoretical maximum density values in Table 2.

Table 3. Mixing theory results (PBX predictions) compared to experimentally measured values. The single component values listed were found experimentally (error ± 0.2 and ± 0.01 for real and imaginary components, respectively) and used in the analysis.

Material	ϵ' (2.5 GHz)	ϵ' (13.3 GHz)	ϵ'' (2.5 GHz)	ϵ'' (13.3 GHz)
TATB	4.5	4.7	< 0.01	< 0.01
HMX	3.4	3.4	0.02	< 0.01
RDX	3.6	3.5	0.02	< 0.01
Viton A	2.5	2.5	0.09	0.09
Kel-F	2.3	2.3	0.02	0.02
Estane:BDNPA/F (1:1)	4.0	4.0	0.38	0.38
BDNPA/F ^{a)}	15.4	N/A ^{b)}	2.79	N/A ^{b)}
PBX 9501 (exp)	3.7	3.9	0.04	0.03
PBX 9501 (predicted)	3.4	3.4	0.04	0.03
PBX 9502 (exp)	4.2	4.6	0.01	< 0.01
PBX 9502 (predicted)	4.4	4.5	< 0.01	< 0.01
PBXN-5 (exp)	3.6	3.6	0.02	< 0.01
PBXN-5 (predicted)	3.3	3.3	0.02	0.01
PBX-RDX (exp)	3.6	3.6	0.02	< 0.01
PBX-RDX (predicted)	3.5	3.4	0.03	0.01

a) BDNPA/F is a liquid at room temperature. These values were taken from the broadband coaxial data. b) Data not valid above approx. 3 GHz due to high permittivity material allowing propagation of higher order modes. See Supporting Information for more discussion.

3.2 Mixing Theory

We used the linear law approximation to determine if the relationship between the permittivity of the individual components of the formulation could be predicted for the overall mixture [5, 18].

$$\epsilon_{\text{eff}} = f\epsilon_i + (1-f)\epsilon_e \quad (11)$$

where ϵ_{eff} is the effective permittivity of the mixture, ϵ_e is the permittivity of the background medium (i.e. explosive material), ϵ_i is the additive permittivity (i.e. binder/plasticizer material), and f is the volume fraction of the additive. We chose this general model because the PBX systems we analyzed have low dielectric contrast, the inclusions are not of a finite geometry, and the volume fraction argument alone is valid. The PBX samples are predominately composed of solid organic explosive crystals (of varying morphology) held together with a polymeric binder network. Eqn 11 was used to compute the predicted ϵ_{eff} values using the experimentally measured values of the individual components at 2.5 and 13.3 GHz; these were then compared to the actual measured values of PBX-RDX, PBX 9502, PBX 9501, and PBXN-5. The values for the individual components that were measured, as well as the measured and predicted values for the formulations, are given in Table 3. The full broadband spectrum for BDNPA/F (liquid at room temperature) is given in the Supporting Information. For all samples we found that the predicted values fall well within the error range of the experimentally determined values; thus the linear law approximation is an appropriate model to predict the effective permittivity of PBX compounds when the values for the individual components are known.

The linear law approximation for mixing may also be used to determine the effective permittivity of solid particle-air mixtures [1, 19]. This is an important method for predicting the permittivity value of a solid material, or the value at a specific density that is unable to be measured experimentally. Powders may be treated as a two-component mixture with air as the background material and the solid powder as inclusions. As long as the permittivity contrast between air and the powder is small, and the sample is at approx. 75% TMD and above, the linear mixing model will give an appropriate prediction of permittivity at different densities [5, 18]. Mixtures with more complex features may also be analyzed by other mixing theories, and are discussed extensively by Sihvola [5].

4 Conclusion

We report the microwave dielectric properties (1–18 GHz) of HMX, RDX, TNT, TATB, PETN, Octol, Comp B, PBX-RDX, PBX 9404, PBXN-5, PBXN-7, PBXW-14, PBX 9501, and PBX 9502 using a twofold experimental approach. The combination of a resonant cavity perturbation technique for determining the dielectric response at discrete frequencies (2.5 and 13.3 GHz) and a wide band (1–18 GHz) open circuit method provides an accurate, broadband measurement. The role of density was explored by measuring the single frequency response at 2.5 GHz on a select number of samples pressed at three different densities. We found that the variation of real permittivity with density is linear with materials having similar slopes, although some formulations (especially those containing a plasticizer component) appear to have a more dramatic density dependence (increased slope). The linear-law dielectric mixing approximation was used to correlate the experimental results of

single-component samples (HMX, TATB, RDX, Kel-F, Viton A, Estane, and BDNPA/F) with the calculated effective permittivity of solid-solid mixtures (i.e. explosive-binder systems) at 2.5 and 13.3 GHz. These calculated values were compared to those found experimentally for several polymer-bonded explosives (PBX). We observed that the results of the predictive model lie well within error of the experimentally measured values for the four formulations we studied. These dielectric properties therefore provide the quantitative information required for accurate computational prediction of the electromagnetic (reflection, transmission, absorption) and thermal response (including direct thermal ignition) of these materials to radiation exposure in this frequency range.

Moving forward, we are exploring the specific effect of adsorbed water on the dielectric behavior of not only TATB, but other explosive solids as well, in addition to the behavior of many of these materials at elevated temperature.

Acknowledgments

This work was funded by the DOE Laboratory Directed Research and Development Program, the Joint DoD/DOE Munitions Program, and the Joint Insensitive Munitions Technology Program. The authors would like to thank Michael D. Janezic (NIST Boulder) for helpful discussions and experimental advice, and Dan Lanterman (NSWC-IHD) for providing samples. We would also like to acknowledge Alan M. Novak (LANL) for illustration and machining assistance, and David M. Oschwald for technical help. LA-UR-13-21819

References

- [1] B. B. Glover, W. L. Perry, Microwave Properties of TATB Particles from Measurements of the Effective Permittivity of TATB Powders, *Propellants Explos. Pyrotech.* **2009**, *34*, 347–350.
- [2] K. Hasue, M. Tanabe, N. Watanabe, S. Nakahara, F. Okada, A. Iwama, Initiation of Some Energetic Materials by Microwave Heating, *Propellants Explos. Pyrotech.* **1990**, *15*, 181–186.
- [3] B. C. Glancy, A. Krall, *Automated Microwave Dielectric Constant Measurement System*, Report TR-86-46, Naval Surface Weapons Center, Dahlgren, VA, USA, **1987**.
- [4] G. F. Cawsey, J. L. Farrands, S. Thomas, Observations of Detonation in Solid Explosives by Microwave Interferometry, *Proc. Roy. Soc., London A* **1958**, *248*, 499–521.
- [5] A. Sihvola, *Electromagnetic Mixing Formulas and Applications*, The Institution of Electrical Engineers, London **1999**.
- [6] M. Martinelli, P. A. Rolla, E. Tombari, A Method for Dielectric Loss Measurements by a Microwave Cavity in Fixed Resonance Condition, *IEEE Trans. Microw. Theory Tech.* **1985**, *33*, 779–783.
- [7] D. C. Dube, M. T. Lanagan, J. H. Kim, S. J. Jang, Dielectric Measurements on Substrate Materials at Microwave-Frequencies Using a Cavity Perturbation Technique, *J. Appl. Phys.* **1988**, *63*, 2466–2468.
- [8] L. F. Chen, C. K. Ong, C. P. Neo, V. V. Varadan, V. K. Varadan, *Microwave Electronics: Measurement and Materials Characterization*, John Wiley & Sons Ltd., Chichester **2004**.
- [9] A. von Hippel, *Dielectric Materials and Applications*, Artech House, Boston **1995**.
- [10] J. Baker-Jarvis, M. D. Janezic, C. A. Jones, Shielded Open-Circuited Sample Holder for Dielectric Measurements of Solids and Liquids, *IEEE Trans. Instrum. Meas.* **1998**, *47*, 338–344.
- [11] J. Baker-Jarvis, M. D. Janezic, D. C. DeGroot, High-Frequency Dielectric Measurements, *IEEE Instrum. Meas. Mag.* **2010**, *13*, 24–31.
- [12] P. W. Atkins, *Physical Chemistry*, W. H. Freeman and Company, New York **1986**.
- [13] E. A. Glascoe, L. N. Dinh, W. Small, G. E. Overturf, Moisture Desorption Rates from TATB Formulations: Experiments and Kinetic Models, *J. Phys. Chem. A* **2012**, *116*, 5312–5316.
- [14] J. W. Pyper, H. M. Buettner, C. J. Cerjan, J. S. Hallam, R. J. King, Measurement of Bound and Free Moisture in Organic Materials by Microwave Methods, *Moisture & Humidity 1985 Symposium*, Washington, DC, USA, **1985**, pp. 909–917.
- [15] R. C. Metaxas, R. J. Meredith, *Industrial Microwave Heating*, Peter Peregrinus Ltd., London **1983**.
- [16] C. M. Anderson-Cook, C. M. Borrer, Paving the Way: Seven Data Collection Strategies to Enhance Your Quality Analyses, *Quality Progress* **2013**, *46*, 18–29.
- [17] R. H. Myers, D. C. Montgomery, C. M. Anderson-Cook, *Response Surface Methodology: Process and Product Optimization Using Designed Experiments*, Wiley, New York **2009**.
- [18] A. H. Sihvola, Self-Consistency Aspects of Dielectric Mixing Theories, *IEEE Trans. Geosci. Remote Sensing* **1989**, *27*, 403–415.
- [19] S. O. Nelson, T. S. You, Relationships Between Microwave Permittivities of Solid and Pulverised Plastics, *J. Phys. D Appl. Phys.* **1990**, *23*, 346–353.

Received: March 22, 2013

Revised: October 27, 2013

Published online: December 5, 2013